

4-28-1990

Fracture Toughness and Fractography of Dental Cements, Lining, Build-Up, and Filling Materials

H. J. Mueller

American Dental Association

Follow this and additional works at: <https://digitalcommons.usu.edu/microscopy>



Part of the [Life Sciences Commons](#)

Recommended Citation

Mueller, H. J. (1990) "Fracture Toughness and Fractography of Dental Cements, Lining, Build-Up, and Filling Materials," *Scanning Microscopy*: Vol. 4 : No. 2 , Article 8.

Available at: <https://digitalcommons.usu.edu/microscopy/vol4/iss2/8>

This Article is brought to you for free and open access by the Western Dairy Center at DigitalCommons@USU. It has been accepted for inclusion in Scanning Microscopy by an authorized administrator of DigitalCommons@USU. For more information, please contact digitalcommons@usu.edu.



FRACTURE TOUGHNESS AND FRACTOGRAPHY OF
DENTAL CEMENTS, LINING, BUILD-UP, AND FILLING MATERIALS

H.J. Mueller

Council on Dental Materials, Instruments, and Equipment
American Dental Association, 211 E. Chicago Avenue,
Chicago, Illinois, 60611

Telephone Number: (312) 440-2505

(Received for publication January 11, 1990, and in revised form April 28, 1990)

Abstract

The plane strain fracture toughness (K_{Ic}) at 23°C and the fractography of zinc phosphate and zinc polycarboxylate cements, buffered glass ionomer liner, amalgam alloy admixed glass ionomer build-up material, and glass ionomer, microfilled and conventionally filled bis-GMA resin composite filling materials were analyzed by elastic-plastic short-rod and scanning electron microscopy methodologies. Results indicated that significant differences occurred in their K_{Ic} 's from the lowest to the highest in the following groups of materials, (i) buffered glass ionomer, (ii) zinc phosphate, glass ionomer, zinc polycarboxylate, and alloy mixed glass ionomer, (iii) microfilled resin, and (iv) conventionally filled resin. All materials except the microfilled resin, which fractured via crack jumping, fractured via smooth crack advance. Filler debonding without any crack inhibiting process was related to materials with low K_{Ic} values. The incorporation of either buffering compounds or alloy particles into glass ionomer had no beneficial effect upon fracture toughness. This was in contrast to microfilled and conventionally filled resins where either crack blunting or crack pinning processes, respectively, were likely involved with their increased K_{Ic} 's. For microfilled resin, distinct radial zones positioned around the chevron apex and characterized by plastically deformed deposited material were related to distinct crack jumps that occurred in the load versus displacement behavior. Finally, for the two remaining materials of zinc phosphate and polycarboxylate, particle cleavage and matrix debonding for the former and shear yielding for the latter occurred.

KEY WORDS: Fracture toughness (K_{Ic}), short-rod, chevron-notched, fractography, crack propagation, crack jumping, continuous crack advance, scanning electron microscopy, restorative composites and cements, particle-matrix debonding, crack pinning and blunting, cleavage, shear yielding.

Introduction

Materials utilized in dentistry for the cementation of inlays, crowns, brackets, etc., for the build-up of cavity preparations, and for the filling of preparations need to be resistant to mechanical fracturing from the forces encountered during biting. Applications involving incisal edges, cusps, and posterior uses are mainly involved. Base and lining materials must also be resistant to the forces generated during the placement of restorations, such as during the condensation of amalgam. Numerous materials are available for these purposes, including zinc phosphate, zinc polycarboxylate, glass ionomer, composite resin, and others.

Strength and modulus of elasticity have long been taken as indicators for the usefulness of dental materials. Recently, the plane strain fracture toughness (K_{Ic}) for a variety of dental materials including composite resin [13, 17], glass ionomer [13, 17], and calcium hydroxide [18], as well as denture base resin [23], bonding resin [17], silicate [17], porcelain [19] and amalgam [20] has been utilized as an indicator for the ease or difficulty in propagating cracks through the materials. Materials with lower K_{Ic} 's are capable of absorbing less mechanical energy prior to fracture than materials with higher K_{Ic} 's.

Microscopy analysis of the fractured surfaces (fractography) has characterized the initiation sites [18] and propagation features [9-11, 17] that occurred during the fracturing process of various dental material structures. For unfilled bis-GMA fracture via a stick-slip process led to arrest lines, while fracture via a continuous process lead to smooth fractured surfaces [9]. For the most part, fracturing of composites has been related to matrix fracture, although the coarseness of fractured surfaces has also been related to particle-matrix debonding and to filler particle fracture [10, 11, 17]. With microfilled composites, prepolymerized filled resin block-matrix debonding may also occur [10].

The purpose of this project was to define the fracture behavior for a variety of dental materials used for cementation, lining, build-up, and filling. Zinc phosphate and polycarboxylate cements, buffered glass ionomer lining material, amalgam alloy admixed glass ionomer build-up material, and glass ionomer and composite resin filling materials were evaluated. The short-rod plane strain fracture toughness of the materials was determined which in turn was followed by scanning electron microscopy (SEM) analysis of the fractured sample halves.

Table 1: Identification of Materials

Material Type	Product Name	P/L ratio*	Manufacturer
<u>Cement</u>			
zinc phosphate	Modern Tenacin	1.0/0.38	L.D.Caulk
polycarboxylate	Durelon	1.0/0.66	Premier
<u>Liner</u>			
buffered glass ionomer	Zionomer Liner	1.0/0.66	Den-Mat
<u>Build-up</u>			
alloy glass ionomer	Miracle Mix	1.0/0.33	GC International
<u>Filling</u>			
glass ionomer	GC Fuji Type II	1.0/0.37	GC International
conventional composite	Compact	1.0/1.0**	Svedia
microfilled composite	Finesse	1.0/1.0**	Caulk/Dentsply

*by wt/wt except for Tenacin which is by wt/vol; **ratio of resin paste to catalyst paste by weight

Table 2: Fracture Toughness
Preliminary data with 6.35 mm diameter samples

Material	K_{Ic} (MPa.m ^{1/2})
Zionomer	0.26
Tenacin	0.43
Fuji Type II	0.41
Durelon	0.30
Miracle Mix	0.30
Finesse	0.74
Compact	1.14

Materials and Methods

Materials

Table 1 identifies the materials, their mixing ratios, intended applications, and their manufacturers. Even though listed for a cementing application, Durelon and Tenacin are also used for base and build-up applications. For these uses the P/L ratio may be increased to 3/1 by weight for Durelon and to a ratio corresponding to a thick putty-like consistency for Tenacin. All ratios listed as well as mixing procedures and mixing times used followed manufacturers' instructions.

Fracture Toughness

Samples. Figure 1 shows a schematic of the sample geometry used for fracture toughness evaluations. The nomenclature of B, W, and a_0 define, respectively, diameter, length and distance from the end face to the chevron apex. Two B sizes, 6.35 (0.03) and 11.28 (0.05) mm were used. The corresponding W dimensions of 1.5B were 9.53(0.06) and 16.92 (0.10) mm, and a_0 dimensions of 0.531B were 3.37 (0.06) and 5.99 (0.08) mm, respectively [4]. The a_0 dimensions have taken into account the fact that the application of the load as given below contacted the inside of the specimen grip grooves at a finite and constant distance from the end surface. Furthermore, with the chevron-notched sample geometry, there is no need to initially form a starter crack as is needed with most other fracture toughness tests. The a_0 dimension can be thought of as the initial crack length.

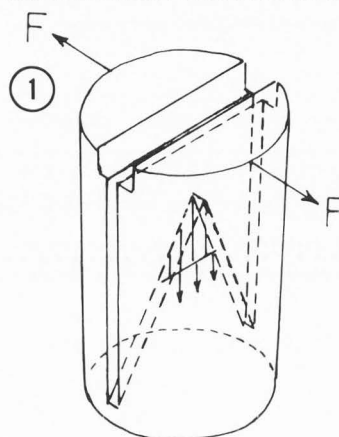


Figure 1. Schematic diagram of the short-rod sample.

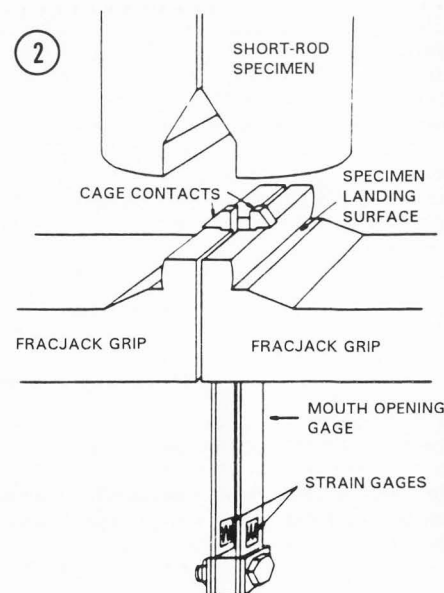


Figure 2. Schematic diagram of sample being positioned onto Fractometer II machine. End groove of sample is positioned onto split collar of load cell and contacts of mouth opening gage.

Following mixing, the unset materials were placed into a stainless steel mold ground to an inside diameter of 11.280 mm, and placed under a load of 100 kg for 10-15 minutes via ground steel plungers positioned into both ends. All samples were stored at 25°C and 100% relative humidity for 1-2 weeks prior to testing. The samples were never allowed to dehydrate. The samples were ground to length on wet SiC abrasive papers and ground by diamond wheels with water as coolant with a Fractometer specimen saw model 4901 (Terra Tek) in forming the grip end groove and chevron slots. The grip end groove for both sample sizes measured 1.97 mm wide by 1.73 mm deep, the chevron slots 0.18 mm wide, and the chevron angle 56°. Note that the end groove was of a square design as shown in Figure 1 and not of an alternative tapered form, as shown in Figure 2. All pertinent dimensions were accurately measured with a depth micrometer and vernier dial calipers as well as with an angle gage and a protractor for measuring the chevron angle. A correction factor C_c was applied in calculating K_{Ic} for deviations in the B, W, and a_0 dimensions by up to 3x the allowed tolerances [10].

Short-rod Testing Methodology. The plane strain fracture toughness (K_{Ic}) at 23°C was determined by utilizing a stand alone Fractometer II model 2101A machine (Terra Tek). Short rod samples, either 6.35 mm or 11.28 mm in diameter, prepared as described above were positioned mouth down onto a split collar of the load cell-mouth opening gauge arrangement, referred to as a Frackjack, as part of the Fractometer instrument shown in Figure 2. The grips on the Frackjack are slightly crowned so that they contact the inside of the specimen grip grooves at a specified depth below the end face. The contact depth is very easily and accurately repeatable by simply placing the specimen onto the Frackjack grips, where gravity holds it in place until the grips come in contact with the grip groove. A three-pronged specimen mouth opening gauge automatically slides into the mouth of the specimen as the specimen is placed onto the grips. Alignment consists of centering the specimen on the grips so the mouth opening gauge hangs free through the slots in the grips, touching nothing except the inside of the specimen mouth. The pivot axis of the Frackjack assures that the rotation of the grips during the test approximates the rotation of the specimen grip groove surfaces as the specimen mouth is forced open. This feature minimizes any changes in the position of the load line that may otherwise occur by the contact point of the crowned grips "walking up" the insides of the grip grooves. During testing, the split collar is separated at a constant preset rate thus applying a tensile shear force (mode I) along the chevron plane. Crack "pop in" and propagation takes place from the apex of the chevron plane. Plane strain conditions are maintained so long as the crack propagates in a longitudinal direction in a manner that forms two symmetrical sample halves. Deviations from this pattern infer the inclusion of a plane stress component. The opening load versus mouth opening displacement of the samples was plotted on an x-y recorder. Calibration of the mouth opening gauge to recorder movement was by matching the movement of the gauge as controlled by a precision micrometer to the actual movement of the recorder pen. Strain rates were determined by

dividing the displacements of the mouth opening gauge obtained from the load versus displacement plots by the corresponding times. The loading rate control of the Fractometer machine was set on the third major division (7 in all) for all 11.28 mm diameter samples and on the first division for all 6.35 mm diameter samples.

Calculation procedures. The plane strain fracture toughness (K_{Ic}) was established by elastic-plastic methodologies [1, 2]. For a smooth crack advance,

$$K_{Ic} = (A) (F_c) (C_c) (1 + p) / B^{1.5} \quad (1)$$

where A is a dimensionless calibration constant independent of material and size and dependent only on sample geometry, F_c is the force corresponding to a crack of critical length a_c , p the plasticity between two unloading-reloading cycles and defined as the ratio of displacements at $F = 0$ and at the average force between the two cycles, C_c a correction factor for dimensions deviating from nominal sizes, and B is the diameter. Hence, any measurement of crack length developed during the test does not enter into the calculation. Currently, the most accurately established value for A is 22.0. For valid tests, unloading-reloading should occur within certain slope ranges. The first unloading-reloading slope ratio r_1 , defined as the ratio of the loading slope to the initial loading slope, should comply with $0.67 < r_1 < 0.58$, while the second reloading slope ratio r_2 should satisfy $0.45 < r_2 < 0.30$, and with $r_2 < 0.7 r_1$. The intersection of the load versus displacement plot with an r_c of 0.55 defined F_c . Only when a test follows ideal linear elastic fracture mechanics (LEFM) does F_c relate to the peak load. Furthermore, plasticity should be less than 20%. For a crack jump advance,

$$K_{Ic} = A_r (F_J) C_c / B^{1.5} \quad (2)$$

where A_r is a calibration constant (between 22-24) relating calibration to crack length [24] and F_J is peak load needed to initiate a crack jump. For valid tests, the slope ratios for the crack jumps, r_J , should satisfy $0.75 > r_J > 0.40$. The calculated K_{Ic} 's were analyzed statistically by analysis of variance procedures. When significance was established, Duncan's multiple range test was used to determine which means were significant [22].

Fractography Analysis

Immediately after testing, the sample halves were placed in a humidior until SEM analysis commenced. Prior to SEM analysis, the 6.35 mm diameter fractured sample halves were mounted with resin on SEM aluminum stubs and sputtered coated with about a 10 nm thick gold film. The fractured surfaces were analyzed with a Tracor Northern ISI SR 50 scanning electron microscope.

Results

Fracture Toughness

Preliminary with 6.35 mm diameter samples. The average K_{Ic} data from three valid tests per material with the loading rate control of the Fractometer machine set on position 1 is presented in Table 2. Strain rates were estimated to be 10-20 times slower than the experimentally determined strain rates for the 11.28 mm diameter samples with

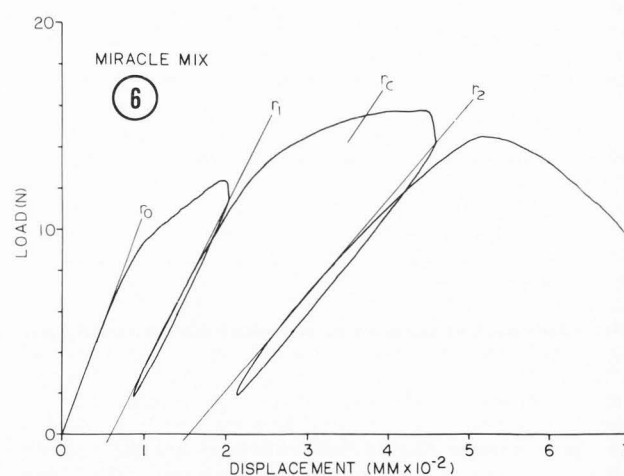
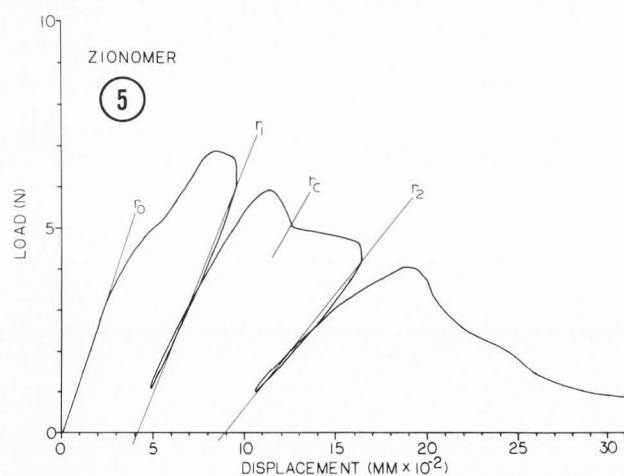
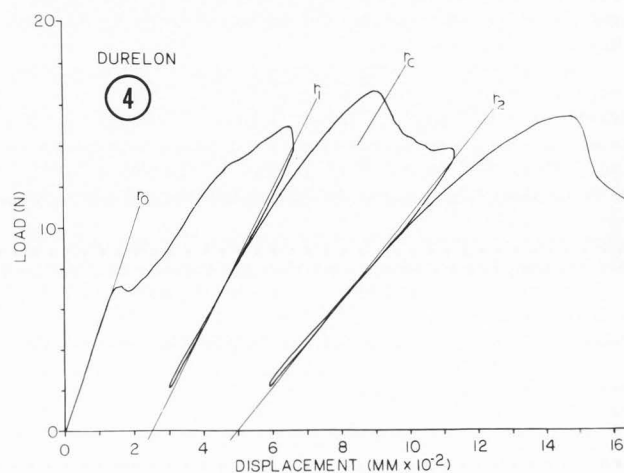
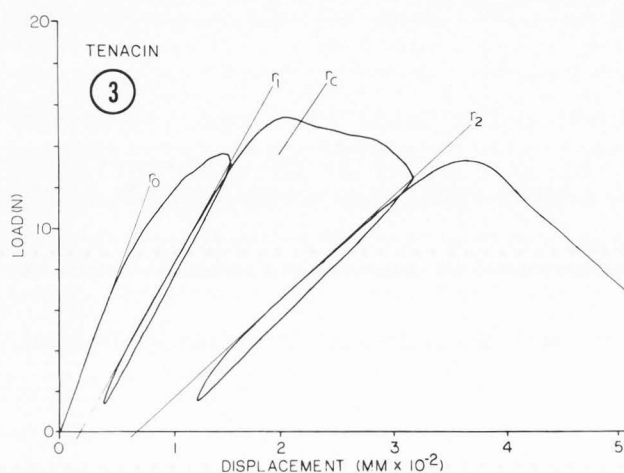
Table 3 Fracture Toughness* Data With 11.28 mm Diameter Samples

Material	n_t	n_{ps}	$F_c(N)$	$F_{max}(N)$	$K_{1c}(MPa.m^{1/2})^{**}$		
					$p = 0$	$p = p$	p
Zionomer	7	4	5.31 (1.30)	6.83 (2.38)	0.099 (0.024)	0.149 (0.037)	0.49 (0.03)
Tenacin	9	7	12.70 (1.91)	13.51 (1.30)	0.234 (0.035)	0.308 (0.031)	0.32 (0.10)
GC Fuji II	12	9	13.89 (2.42)	15.34 (2.24)	0.257 (0.047)	0.379 (0.056)	0.48 (0.15)
Durelon	6	6	14.20 (1.73)	16.12 (0.89)	0.264 (0.033)	0.391 (0.051)	0.48 (0.05)
Miracle Mix	6	4	14.71 (2.58)	15.52 (2.80)	0.275 (0.049)	0.380 (0.059)	0.46 (0.05)
Finesse***	6	6	eq. 2 used	46.77 (2.89)	0.685 (0.070)	eq. 2 used	0.04 (0.03)
Compact	6	5	65.51 (0.91)	66.16 (1.08)	1.226 (0.038)	1.116 (0.049)	-0.09 (0.03)

*means and standard deviations; a dotted line connecting means signifies no significance at the 99% level.

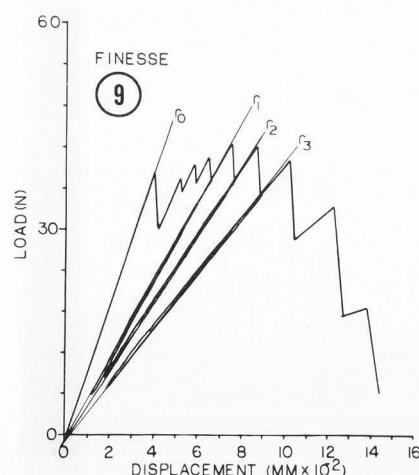
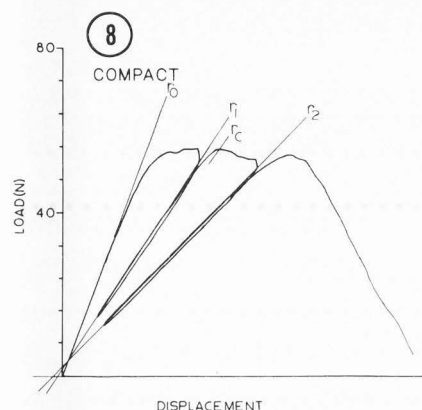
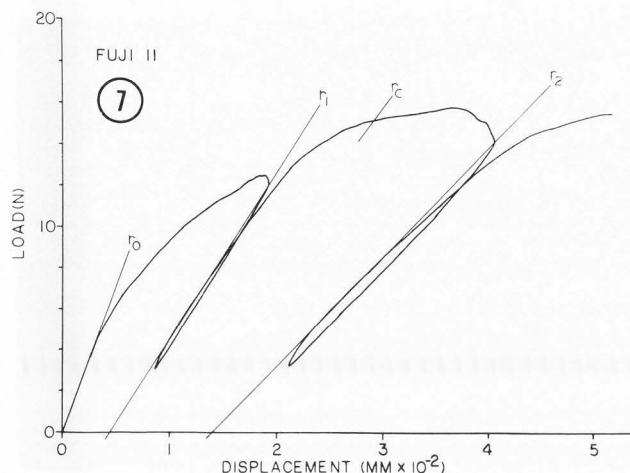
**fracture via smooth crack advance (eq 1) except for Finesse which fractured via crack jumping (eq 2).

***a total of 18 distinct crack jumps included with the mean K_{1c} .



the loading rate control set on position 3. Finesse fractured via a crack jump process while all other materials fractured via a smooth crack advance. Some difficulty was encountered with a number of the materials of this sample size and with low fracture toughness in being positioned without

damaging onto the split collar of the load cell prior to testing. Both composite materials, however, presented much less difficulty in this regard and provided accurate representative load versus displacement plots.



Figures 3-9. Applied load versus mouth opening displacement for:

Figure 3: Tenacin; Figure 4: Durelon;
Figure 5: Zionomer; Figure 6: Miracle Mix;
Figure 7: GC Fuji II; Figure 8: Compact*;
Figure 9: Finesse.

*See Discussion with Editor on the last page.

Table 4. Transducer Displacement Calibration

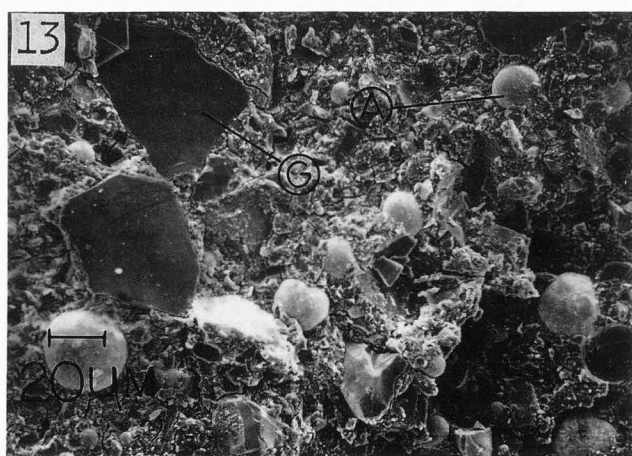
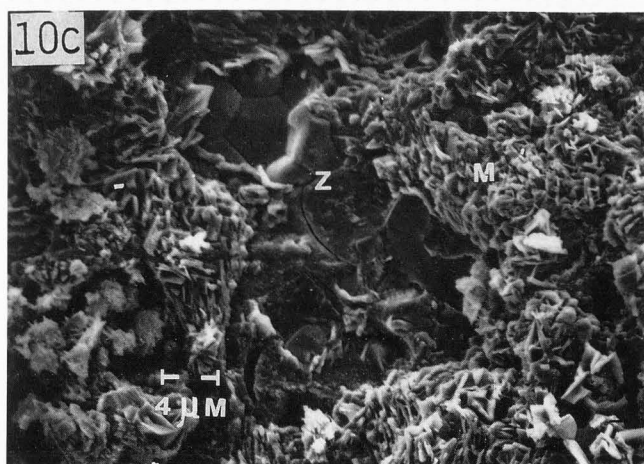
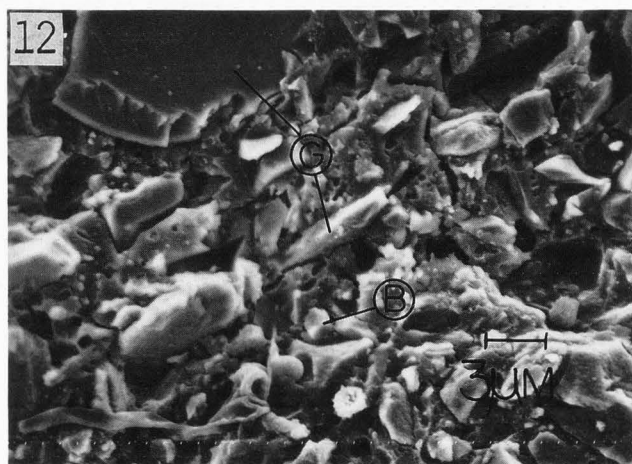
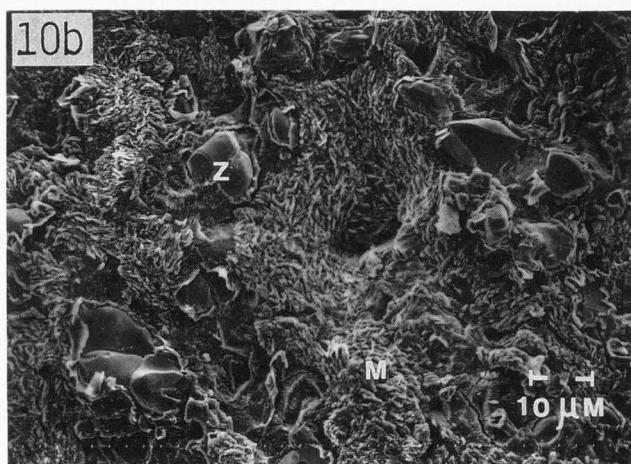
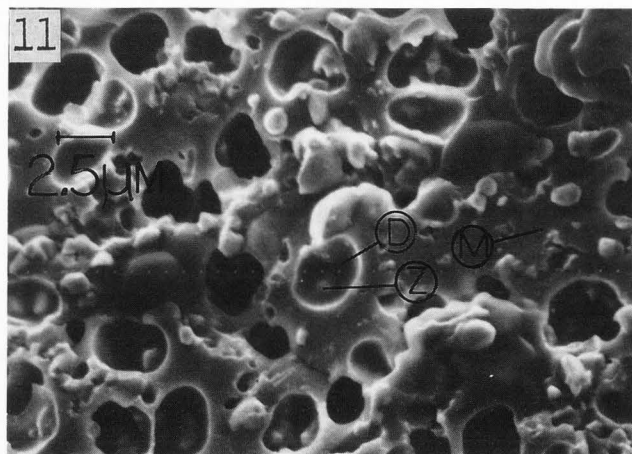
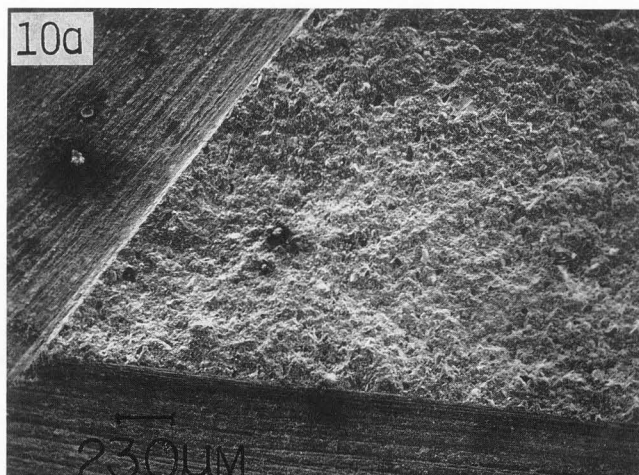
Material	mm/250 mm chart*
Zionomer	0.217 (0.148)
Tenacin	0.035 (0.017)
GC Fuji II	0.039 (0.014)
Durelon	0.118 (0.013)
Miracle Mix	0.052 (0.006)
Finesse	0.188 (0.026)

*corresponds to strain rates of $0.9-1.5 \times 10^{-3}$ mm/sec.

11.28 mm diameter samples. Figures 3-9 present load versus mouth opening displacement plots for Tenacin and Durelon cements, Zionomer liner, Miracle Mix build-up material, and GC Fuji II, Compact and Finesse filling materials, respectively. All plots except for Finesse are characterized by a smooth crack advance. Finesse revealed a crack jump behavior, without exception in all samples with both sizes evaluated. The smooth crack advance plots revealed an initial region where the load increased linearly with displacement, by a region where "pop-in" of the crack at the apex occurred, where the load increased non-linearly with displacement, and where the load decreased from a peak load value non-linearly with displacement. A sudden reduction in load often times out of range in the figures, was characteristic of instantaneous crack propagation resulting in catastrophic failure. Durelon, Finesse, and Compact showed a high percentage of plane strain fractured samples, while Zionomer, GC Fuji II, and Miracle Mix showed a lower percentage. Tenacin also fractured with good plane strain constraints. Table 3 presents the means and standard deviations of the results. Included are the number of samples tested (n_t), the number of samples that fractured under plane strain conditions (n_{ps}), the maximum force generated in the load-displacement plots (F_{max}), the force (F_c) corresponding to a crack of critical length, K_{IC} at $p = 0$ and at $p = p$, and the measured plasticity p . Analysis of variance indicated that there was significance at the 99% level of confidence among the different materials for F_{max} , F_c , K_{IC} at $p = 0$ and $p = p$, and p . Further analysis showed significant groupings as shown in Table 3. A line connecting means signifies no significance.

Table 4 presents the results obtained for the calibration of the mouth opening gauge with respect to the movement on the recorder as well as for the ensuing strain rates with the loading rate control of the Fractometer set on the third major division.

Fractography Analysis. Figures 10a-c, 11, 12, 13, 14, 15a-b, and 16a-c present SEM fractographs for zinc phosphate, polycarboxylate, buffered glass ionomer, amalgam alloy admixed glass ionomer, glass ionomer, conventional composite, and microfilled composite, respectively. The mating fracture surfaces of the samples appeared similar to these fractographs. In addition, most of the lower magnification fractographs showed a slight distinction in appearance towards the bottom of the chevron plane. A somewhat coarser structure usually occurred which corresponded to the region on the load versus displacement curve where the load dropped suddenly. For the micrographs presented, only surface texture within the stable crack growth regions are shown.



Figures 10 - 13. SEM fractographs of: **Figure 10.** Tenacin at low magnification (**a**) showing apex and about 75% of the chevron plain strain fracture plane, and at higher magnifications (**b** and **c**). "Z" particles are unreacted zinc oxide particles fractured by cleavage, and "M" particles are the zinc phosphate matrix crystals fractured by cleavage or debonded by decohesive rupture. **Figure 11.** Durelon. Dimples "D" have been formed by coalescence of microvoids by a shear yielding process, "Z" particles are unreacted zinc oxide, and "M" is zinc polycarboxylate matrix. **Figure 12.** Zionomer. "G" particles are glass particles and "B" particles are buffering additives, such as, zinc oxide, calcium fluoride, and others. **Figure 13.** Miracle Mix. "G" particles are glass particles and "A" particles are Lumina amalgam alloy spherical additive.

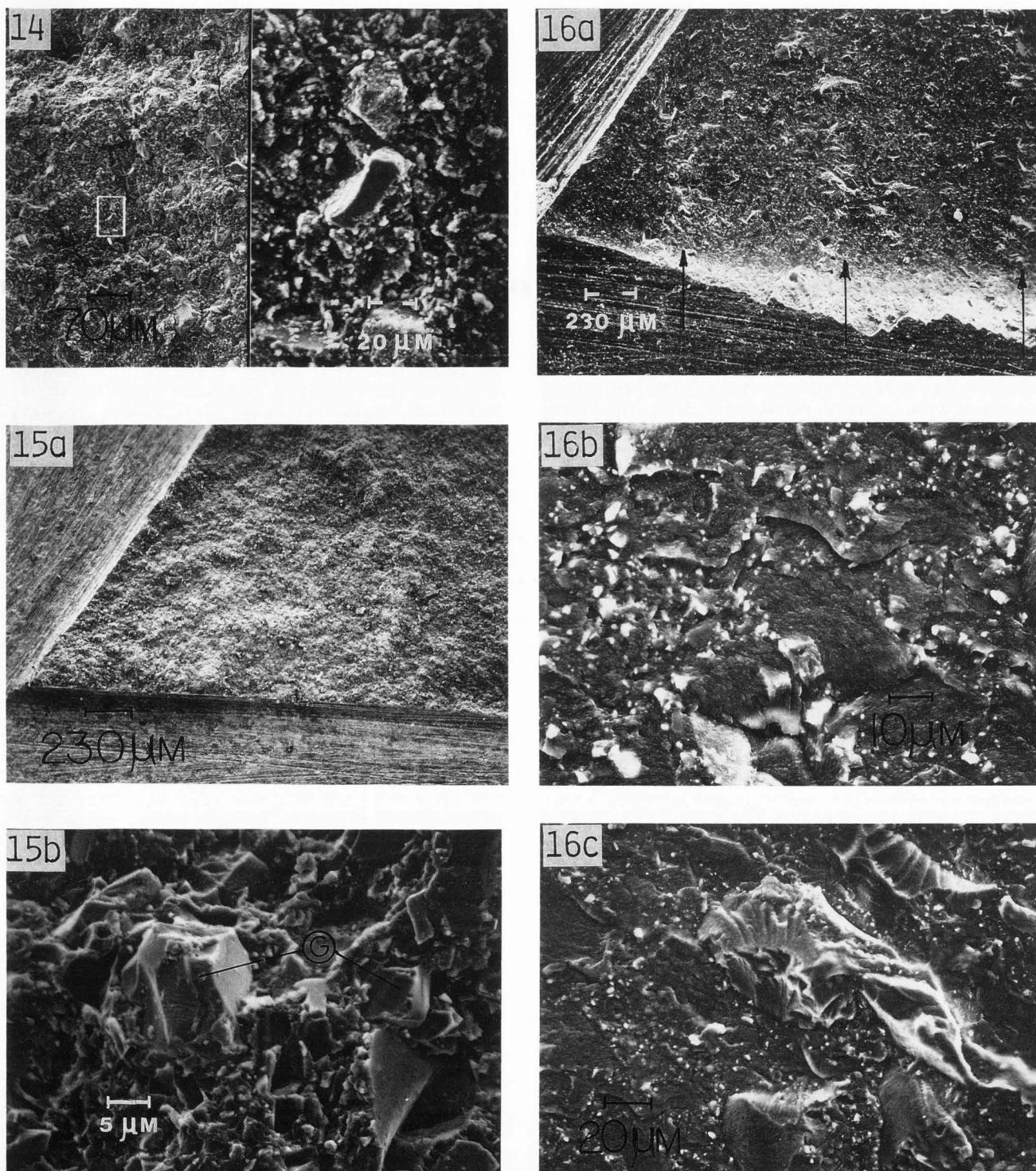


Figure 14. SEM fractograph of Fuji Type II. All particles are composed of glass.

Figure 15. SEM fractographs of Compact at low magnification (a) and at higher magnification (b) showing particle-matrix debonding and particle cleavage fracture of glass "G" particles.

Figure 16. (a) SEM fractographs of Finesse at low magnification showing regions of material denoted by arrows that are microstructurally different than rest of surface. Higher magnification of surface in between arrows (b) shows fractured surface with numerous steps while of material at the arrows (c) shows fractured surface overlaid with deposited material.

Glass ionomer. For glass ionomer material, cohesive rupture debonding glass particles was the primary fracture process. Several isolated larger-sized particles fractured via cleavage. It appeared that less particles were cleaved than with the other forms of the glass ionomer material. Some of the seemingly debonded particles, especially the smaller ones, contained a resinous layer which indicated that the fracture path ran through the matrix at a short distance from the particles, in contrast to the modified glass ionomer materials investigated. Numerous cracks occurred through matrix, a characteristic feature of glass ionomer materials. If indeed these were craze cracks, then the molecular weight of the polymer chains, degree of cross linking, and orientation would have had a profound effect upon the ease or difficulty in their formation. Increased molecular weight and cross linking would have been expected to make craze formation more difficult. It is doubtful, though, that any degree of ordering of molecules occurred with these materials. Micro-deformation mechanisms associated with semi-crystallinity of polymers would not be expected to play an important role [19]. The degree of hydration would have had a profound effect. However, the samples were never allowed to dehydrate, even during testing. The possibility exists, though, that dehydration and cracking could have occurred immediately before SEM analysis (during sputter coating) or during SEM analysis itself.

Conventional composite. For conventional composite resin, debonding of both larger-sized and smaller-sized filler silica particles was the primary fracture process. Numerous depressions in the matrix, where particles have been removed, were evident. Debonding of filler particles in composites has been previously reported [10, 11, 17]. The main mode of crack propagation in all composites investigated was through the matrix and along the filler/matrix interface [11]. In another report [17], however, distinction of filler and matrix was often times difficult because of a layer of resin adhering to filler. This implies that the cracking process has been mainly in matrix at short distances from filler particles. This latter situation can be generated by stress fields set-up around filler particles which interact with the propagating crack. The size, shape, and loading of the filler can affect the stress fields set-up around the dispersed particles in accommodating a crack.

Increased K_{IC} for conventional composite was likely due to mechanisms such as crack pinning or crack blunting [7]. In crack pinning the filler particles act as obstacles to the propagation of the crack and force the crack to bow, analogous to the concept used in the dislocation theory for the precipitation hardening of alloys [5]. With a crack blunting mechanism, debonding of particles occurs ahead of the crack tip causing blunting of the crack, analogous to the concept used to explain the strain hardening of metals by the coalescence of microvoids with the crack tip [5]. Because crack blunting processes usually involves a stick-slip type of crack propagation [5, 8], it appears that with conventional composite a crack pinning mechanism was operative. Another approach being developed to predict the speed and direction of the passage of a crack through a multiphase material is based upon the concept of a mesophase, a third phase which represents

the interface or contact [6].

Microfilled composite. For microfilled resin, which was characterized by a crack jump mode of fracture in the load versus displacement behavior, three radial bands (arrows in Figure 16a) of a different surface topography occurred around the chevron apex and with each zone corresponding exactly to one of the peak loads just prior to a crack jump. These zones were identified to contain heaps of material very likely highly deformed plastically and deposited during the cracking process. These observations were totally consistent with the concept of crack blunting presented earlier by the formation of a plastic zone ahead of the crack tip [9]. A slightly different interpretation has also been made with this process [7]. Here crack blunting is thought to occur by decohesion of particles from the matrix in front of the crack as the crack is propagating. Hence, the sample must essentially be reloaded to initiate a new sharp crack. This latter interpretation seems unlikely in the present situation if submicron size particles were considered as the entity being debonded. If however, the prepolymerized filled resin blocks and resin matrix became debonded, as has been suggested earlier [10], then a better rationale can be made with the interpretation of the microstructures in Figures 16b and c. Clearly, the underlying surface in Figure 16c appears to be made-up of numerous individual regions, very likely the prepolymerized filler blocks. Similarly, the overlaid material can be thought to consist of similar blocks of plastically deformed material. The material in between the zones (Figure 16b) may also consist of layers comprising individual filler blocks.

Conclusions

1. Significant differences existed in the fracture toughness among four groups of materials, these being from the lowest to highest, (i) Ziommer liner; (ii) Tenacin, GC Fuji II, Durelon, and Miracle Mix; (iii) Finesse; and (iv) Compact.
2. All materials except Finesse fractured via a smooth crack advance during evaluation of their short-rod fracture toughness by means of an elastic-plastic method. Finesse fractured via a crack jumping process.
3. For low K_{IC} materials including groups (i) and (ii) above, less difficulty was experienced with the techniques of testing by using 11.28 mm instead of 6.35 mm diameter samples, even though the smaller diameter gave similar values.
4. A micromechanical mechanism debonding filler particles from matrix and occurring without any crack inhibiting process correlated to the lowest K_{IC} . Buffered and amalgam alloy particles in glass ionomer materials provided no beneficial effect in regard to improving their fracture toughness.
5. The higher K_{IC} values for Compact and Finesse were thought to be due to crack pinning and crack blunting processes, respectively. Compact fractured mainly through matrix with particle debonding and fracture occurring only limitedly. Debonding of prepolymerized filler blocks from resin matrix was thought to be involved with the fracture of Finesse. Each crack jump on the load versus displacement diagram for Finesse correlated to a radial zone of material emanating around the chevron apex and contained overlaid plastically deformed material.

6. Durelon fractured via a shear yielding process. Here shear stresses were generated at zinc oxide particle inclusions which in turn formed numerous voids, while Tenacin fractured via cleavage of unreacted particles and debonding of phosphate matrix crystals.

Acknowledgement

Partial support was provided by a grant from the National Institutes of Dental Research, No DE 05761.

References

1. Barker LM. (1979). Theory for determining K_{Ic} from small, non-LEFM specimens, supported by experiments on aluminum. *Internat J Fract* 15:515-536.
2. Barker LM. (1979). Specimen size effects in short-rod fracture toughness measurements. In: Chevron-Notched Specimens. Underwood JH, Freiman SW, Baratta FI (ed.) ASTM STP 855, American Society for Testing and Materials. Philadelphia, 117-133.
3. Barker LM. (1980). Development of the short rod method of fracture toughness measurement Report TR 80-58, Terra Tek, Salt Lake City, UT.
4. Barker LM. (1981). Short rod and short bar fracture toughness specimen geometries and test methods for metallic materials. In: Fracture Mechanics: 13th Conference. Roberts R (ed.) ASTM STP 743. American Society for Testing and Materials. Philadelphia, PA, 456-475.
5. Bates RC. (1989). Micromechanical modeling for prediction of lower shelf, transition region, and upper shelf fracture properties. In: Fracture Mechanics: Microstructure and Micromechanisms. Nair SV, Tien JK, Bates RC, Buck O (eds.) ASM International, Metals Park, OH, 131-168.
6. Bhattacharya SK. (1986). Metal Filled Polymers. Marcel Dekker, NY, 259-330.
7. Cantwell WJ, Roulin-Moloney AC. (1989). Fractography and failure mechanisms of unfilled and particulate filled epoxy resins. In: Fractography and Failure Mechanisms of Polymers and Composites. Roulin-Moloney AC (ed.). Elsevier, NY, 233-290.
8. Davis DM, Waters NE. (1986). An investigation into the fracture behavior of a particulate filled bis-GMA resin. *J Dent Res* 66:1128-1133.
9. Davis DM, Waters NE. (1989). Fractography of a bis-GMA resin. *J Dent Res* 68:1194-1198.
10. Ferracane JL, Antonio RC, Matsumoto H. (1986). Variables affecting the fracture toughness of dental composites. *J Dent Res* 66:1140-1145.
11. Ferracane JL. (1989). Indentation fracture toughness of and crack propagation mode in dental composites. In: Biomedical Materials and Devices. Hanaker A (ed.) Mat Res Soc Symp Proc Vol 110. Materials Research Society, Pittsburgh, 619-624.
12. Doll W. (1989). Fractography and failure mechanisms of amorphous thermoplastics. In: Fractography and Failure Mechanisms of Polymers and Composites. Roulin-Moloney AC (ed.) Elsevier, NY, pp 387-436.
13. Goldman M. (1985). Fracture properties of composite and glass ionomer dental restorative materials. *J Biomed Mater Res* 19:771-783.
14. Hull D. (1975). Microstructural effects on fracture processes in polymers. In: The Mechanics

and Physics of Fracture. The Metal Society and Institute of Physics, London, pp. 124-130.

15. Kerlins V, Phillips A. (1987). Modes of fracture. In: Metals Handbook 9th ed Vol 12, Fractography. American Society for Metals, Metals Park, OH, pp 12-71.

16. Kuksenko VS, Tamuzs VP. (1981). Fracture Micromechanics of Polymer Materials. Martinus Nijhoff, Boston, pp 139-166.

17. Lloyd CH, Mitchell L. (1984). The fracture toughness of tooth colored restorative materials. *J Oral Rehab* 11:257-272.

18. Lloyd LL, Anderson JN. (1980). The strength and fracture toughness of calcium hydroxide preparations. *J Oral Rehab* 7:155-165.

19. Morena R, Lockwood PE, Fairhurst CW. (1986). Fracture toughness of commercial dental porcelains. *Dent Mater* 2:58-62.

20. Mueller HJ. (1989). Fracture toughness and fractography of dental amalgam. *Microstruc Sci* 18 (accepted for publication).

21. Powell PC. (1983). Engineering with Polymers. Chapman and Hall, NY, pp. 117-153.

22. Rickmers AD, Todd HN. (1967). Statistics: An Introduction. McGraw-Hill, NY pp 154-279.

23. Stafford GD, Huggett R. (1980). Fracture toughness of denture base acrylics. *J Biomed Mater Res* 14:359-371.

24. Terra Tek. (1984). The Fractometer Systems II Manual. Terra Tek. Salt Lake City, UT, p C5.4.

Discussion with Editor

Editor: Why there are no values provided on the x-axis on Figure 8?

Author: In order to adjust the initial loading slopes for each material to the approximate same value of R_0 , a recorder potentiometer is adjusted on the Fractometer machine. Calibration of the mouth opening gauge is dependent on this potentiometer setting. For Compact, the exact potentiometer settings were not kept. Therefore, the exact calibration remains unknown. However, the settings were similar to those used with Finesse (Fig. 9) and therefore similar to the values provided on the x-axis in Fig. 9. This procedure in no way detracts from the calculation procedure for K_{Ic} , since as shown in equation 1, only a plasticity term, p , utilizes the x-axis values. As defined, p is a relative measurement equal to the ratio of the displacements at $F = 0$ and at the average force between the two unloading-reloading cycles.

Editor's Note: All of the other concerns of the reviewers were appropriately addressed by text changes, hence there is no Discussion with Reviewers.